processes

MDPI

Article

Transient Pressure and Temperature Analysis of a Deepwater Gas Well during a Blowout Test

Haiquan Zhong [1,*], Chuangen Zheng [1], Miao Li [1,2], Tong Liu [3], Yufa He [4] and Zihan Li [4]

[1] State Key Laboratory of Oil and Gas Reservoir Geology and Exploitation, Southwest Petroleum University, Chengdu 610500, China; 202022000688@stu.swpu.edu.cn (C.Z.); limiao2021@yeah.net (M.L.)
[2] Sichuan Fortisa Petroleum Technology Development Co., Ltd., Chengdu 610500, China
[3] Research Institute for Engineering Technology, Sinopec Southwest Branch Company, Deyang 618000, China; liutong1.xnyq@sinopec.com
[4] State Key Laboratory of Natural Gas Hydrates, CNOOC Research Institute Co., Ltd., Beijing 100028, China; heyf@cnooc.com.cn (Y.H.); lizh19@cnooc.com.cn (Z.L.)
* Correspondence: swpuzhhq@126.com

Abstract: On one hand, a blowout test can clean the bottom of the well, and on the other, it can learn the productivity of the well, which is important work before putting the well into production and also the main basis for production allocation of the well. The accurate prediction of the blowout test process provides a theoretical basis for the design of a reasonable blowout test system and the determination of well cleaning time. During deepwater blowout tests, gas and liquid flows are unsteady in pipes, and flow parameters change over time. At present, accurately predicting changes in fluid temperature, pressure, liquid holdup, and other parameters in a wellbore during an actual blowout process using the commonly used steady-state prediction methods is difficult, and determining whether a test scheme is reasonable is impossible. Therefore, based on the conservation of mass, momentum, and energy during the blowout test process, in this study, formation, wellbore, and nozzle flows were coupled for the first time, and a time and space of unsteady pressure drop and a heat transfer differential equation system was established; furthermore, using the Newton–Raphson method, the equations were solved. Finally, the simulation of the transient flow of the blowout test was completed. Considering a measured deepwater gas well A as an example, the blowout test process was simulated, and the variations in the wellbore flow parameters were analyzed. Comparing the simulation result with the test data, we concluded the following. (1) During the blowout process, the wellbore temperature gradually increased; pressure at the bottom of the wellbore decreased; and pressure at the wellhead increased; and (2) the established model agreed well with the actual production data, and the average error of the wellhead pressure and temperature was less than 5%. Considering the high production capacity of deepwater gas wells, the use of large-sized tubing and nozzles to spray is recommended, which can improve the speed of clearing wells and prevent the formation of hydrate.

Keywords: deepwater gas well testing; multiphase flow; coupled model of pressure and temperature field; numerical simulation; transient flow

Citation: Zhong, H.; Zheng, C.; Li, M.; Liu, T.; He, Y.; Li, Z. Transient Pressure and Temperature Analysis of a Deepwater Gas Well during a Blowout Test. *Processes* **2022**, *10*, 846. https://doi.org/10.3390/pr10050846

Academic Editors: Chuanliang Yan, Kai Zhao, Fucheng Deng and Yang Li

Received: 28 March 2022
Accepted: 22 April 2022
Published: 25 April 2022

1. Introduction

At present, deepwater is one of the focuses of oil and gas resource development and has broad prospects, but deepwater oil and gas exploitation has been handicapped by the complexity of the environment. Due to environmental complexities in deepwater gas wells, fluid flow parameters change with time during a two-phase flow (i.e., from the formation to the wellbore and in the wellbore), thereby making the flow complicated. Therefore, accurately predicting changes in flow parameters such as wellbore fluid temperature, pressure, and liquid holdup during an actual blowout process is difficult, and researching the two-phase transient flow during blowouts is necessary.

Deepwater well testing is characterized by high technology, investment, and risk. Moreover, gas well testing is crucial in the development potential evaluation of deepwater wells [1,2]. Wellbore storage effect is obvious during a shut-in period of a deepwater gas well [3]. The maximum test flow of the test string, ground process, and test system affect the test, and the influence of the test system is the greatest [4]. Therefore, Wu et al. designed a work system based on a critical test flow and proposed a test program of "one-open and one-close" [5].

At present, the research on wellbore temperature and pressure is relatively perfected. Churchill and Chu studied the convective heat transfer coefficient of seawater, and Mathews conducted a similar study [6,7]. Chin and Wang studied thermodynamic losses in the risers of top test trees [8]. Based on the first principle of transient gas well production, Hasan et al. established a wellbore temperature model [9]. Stiles and Trigg developed a temperature mathematical simulator for deepwater drilling [10]. Izgec et al. and Ismadi used nodal analysis methods to study temperature distribution [11–14].

Spindler explicitly gave the initial and boundary conditions for a calculated transient temperature distribution [15]. Hasan and Kabir unified different situations of heat transfer models, and Kabir used transient measured temperature to calculate static temperature as well as established flow temperature gradient to accurately estimate geothermal gradient and gas flow [16,17]. Chen derived a set of borehole-formation heat transfer differential equations [18]. The difference between seawater and production pipe temperatures was large, and thermal radiation could not be ignored, there was a large difference between the flow of the formation and seawater sections in deepwater wells, and heat loss mainly occurred in the seawater section [19,20].

Liu et al. established a transient temperature and pressure model for gas well testing to explain the reason of abnormal wellhead pressure [21]. Zhang et al. reported that the pressure at the bottom decreased to a certain extent, whereas the pressure at the wellhead gradually increased and finally remained relatively stable. and Kabir et al. studied the production logging of natural gas wells [22]. These studies were based on heat transfer models and recorded well-logging fluid flows along boreholes to determine regional contributions.

With an increase in production, the Joule–Thomson effect increases. On this basis, Li et al. obtained the relationship between temperature and flow rate, and Xu established a coupling model of the transient multiphase flow between the formation and wellbore. He et al. studied the induced transient flow of deepwater gas wells and established a transient model of multiphase flow, reproducing the flow in a wellbore under actual working conditions [23–26].

At present, the commonly used prediction methods do not consider the transient flow process response of formation inflow, wellbore flow rule, and surface nozzle flow. Moreover, the prediction of the blowout test temperature, pressure, and liquid holdup of the actual blowout test wellbore fluid has poor accuracy. Therefore, in a first, herein, the formation, wellbore, and surface nozzle flows are coupled to establish a deepwater wellbore transient flow model of the blowout test to improve the accuracy of the calculation results.

2. Mathematics Model

The wellbore flow is an unsteady two-phase flow in the test. The model is assumed as follows:

(1) the gas–liquid flow in the pipe is one-dimensional and unsteady;
(2) the gas is compressible, whereas the liquid is incompressible;
(3) a high production and homogeneous flow during the blowout test; and
(4) the downward direction of the wellbore flow is defined as the positive direction of the z-axis.

According to the principles of the conservations of mass, momentum, and energy, the control equations are

$$\frac{\partial \rho_m}{\partial t} + \frac{\partial G_m}{\partial z} = 0 \tag{1}$$

$$\frac{\partial G_m}{\partial t} + \frac{\partial}{\partial z}\left(\frac{\partial G_m^2}{\rho_m}\right) + \frac{\partial P}{\partial z} + \rho_m g \sin\theta + \frac{f_m G_m |G_m|}{2 d_{ti} \rho_m} = 0 \tag{2}$$

$$Q = \frac{\partial (mE)_{cv}}{\partial t} + \frac{\partial (m\prime E\prime)_w}{\partial t} + \frac{\partial}{\partial z}\left[w_m\left(H_f + \frac{1}{2}v^2 + gz\cos\theta\right)\right] \tag{3}$$

Considering the high gas production in the test, the transient simulation of the gas–liquid flow is simplified to a homogeneous flow. Rendeiro and Kelso (1988) modified the correction of the gas relative density, and the mixture relative density and mixture density are expressed as follows:

$$\gamma_m = \frac{\gamma_g + 817.7\gamma_L/GLR}{1 + 200GLR} \tag{4}$$

$$\rho_m = \frac{28.96\gamma_m P}{Z_m RT} \tag{5}$$

where the natural gas deviation coefficient, Z_m, can be calculated using the Dranchuk–Abu–Kassem relation:

$$\begin{aligned} Z_m = 1 + \left(A_1 + A_2/T_{pr} + A_3/T_{pr}^3 + A_4/T_{pr}^4 + A_5/T_{pr}^5\right)\rho_{mr} + \left(A_6 + A_7/T_{pr} + A_8/T_{pr}^2\right)\rho_{mr}^2 \\ -A_9\left(A_7/T_{pr} + A_8/T_{pr}^2\right)\rho_{mr}^5 + A_{10}\left(1 + A_{11}\rho_{mr}^2\right)\left(\rho_{mr}^2/T_{pr}^3\right)\exp\left(-A_{11}\rho_{mr}^2\right) \end{aligned} \tag{6}$$

2.1. Steady-State Heat Transfer

Heat transfer in deepwater wells comprises two sections: seawater and formation sections. The heat transfer in the wellbore is steady, and the heat transfer during the formation is unsteady and can be described via a transfer heat-conduction time function. The wellbore structure and length of the differential cell, dz, are shown in Figure 1.

According to the law of heat conduction from the wellbore to formation and unsteady heat dissipation, the radial heat gradient equation of formation can be established. Moreover, according to the law of convection heat transfer from the wellbore to seawater, the radial heat gradient equation of seawater can also be established. Combining the conservation of energy and enthalpy gradient equations, a general formula to calculate the wellbore temperature gradient of offshore oil and gas wells is formed:

$$\frac{dT}{dz} = -L_r(T - T_{ei}) - \frac{g\cos\theta}{C_{pm}} - \frac{v_m}{C_{pm}}\frac{dv_m}{dz} + C_{Jm}\frac{dp}{dz} \tag{7}$$

For the formation section:

$$L_r = \frac{2\pi r_{to} U_{to1} K_e}{C_{pm} w_t [K_e + f(t_D) r_{to} U_{to1}]}$$

If the fluid heat-transfer coefficient in tubing, the heat conductivity of tubing and casing offer negligible resistance to heat flow, U_{to1} can be approximated by

$$U_{to2} = \left[\frac{1}{h_c + h_r} + \frac{r_{to}}{K_{cem}} \ln\frac{r_w}{r_{co}}\right]^{-1}$$

For the seawater section:

$$L_r = \frac{2\pi r_{to} U_{to2}}{C_{Pm} w_t}$$

Similarly, where U_{to2} can be approximated by

$$U_{to2} = \left[\frac{1}{h_c + h_r} + \frac{r_{to}}{r_{co}h_w}\right]^{-1}$$

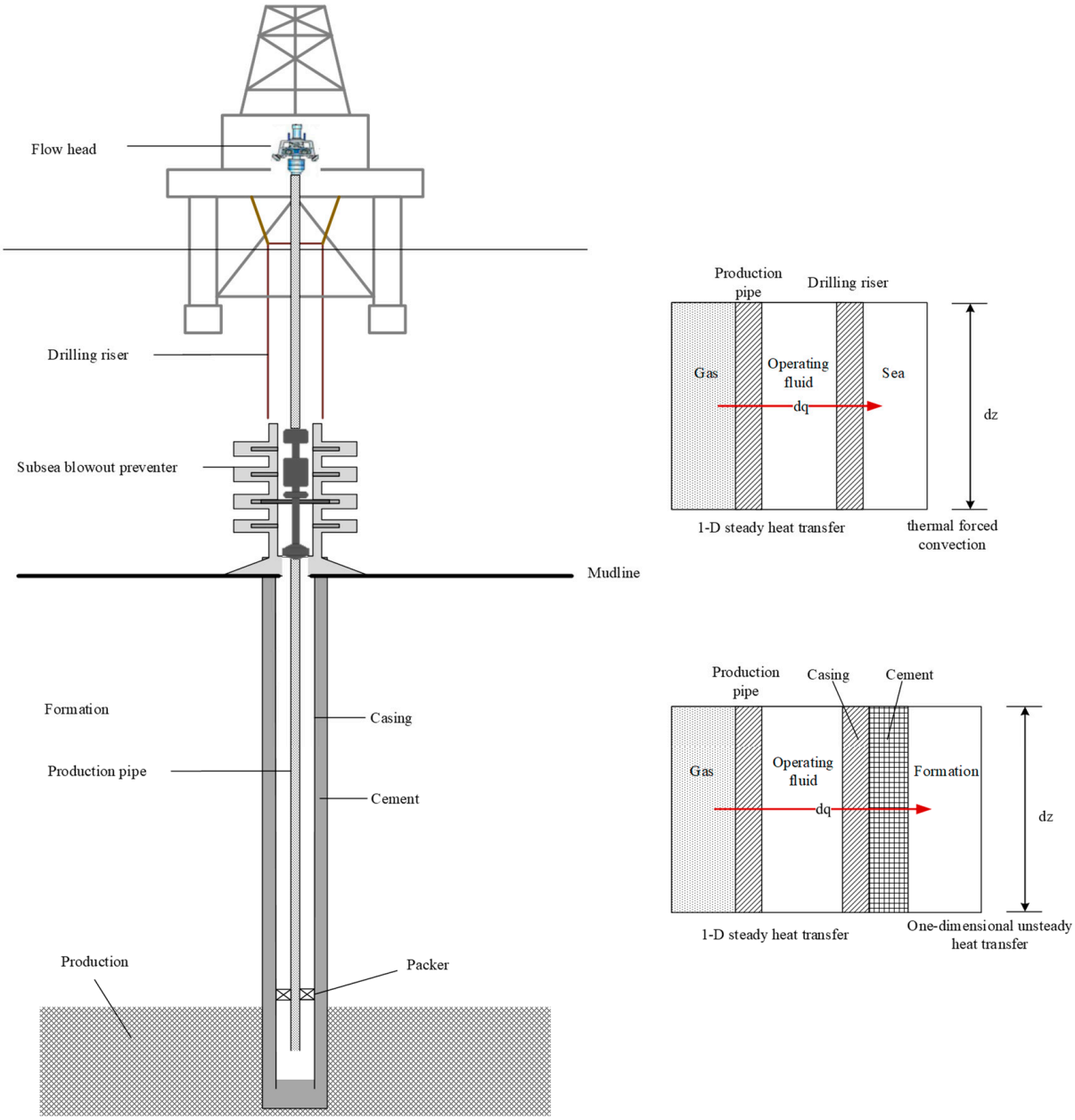

Figure 1. Simplified sketch of deepwater production for a gas well.

2.2. Transient Heat Transfer

During the test, the output fluid dissipates heat to the wellbore, and the temperature decreases gradually from the bottom to wellhead. Furthermore, the cement and string are continuously heated by the high-temperature fluid so that the temperature difference between the fluid and wellbore constantly decreases, and the fluid temperature continuously changes with time. Therefore, the heat loss of the wellbore fluid during the test blowout is a transient process (Figure 2).

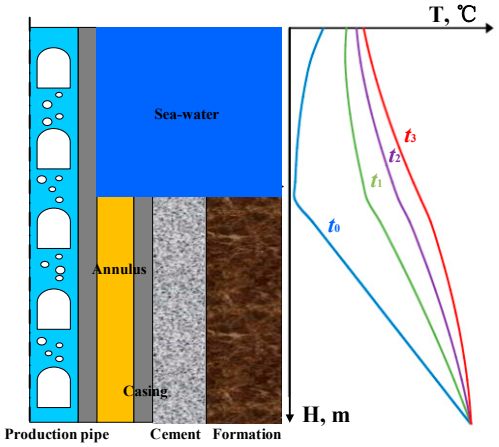

Figure 2. Schematic of the temperature change in the heat transfer fluid of the wellbore.

We introduced the Hasan and Kabir heat storage coefficient into Equation (3) and combined it with the wellbore steady-state heat transfer, Equation (7); an explicit equation for calculating the transient temperature of the wellbore fluid is obtained as follows:

Partial differential equation:

$$Q = \frac{\partial (mE)_{cv}}{\partial T} + \frac{\partial (m'E')_w}{\partial T} + \frac{\partial}{\partial z}\left[w_m\left(H_f + \frac{1}{2}v^2 + gz\cos\theta\right)\right]$$

Introduced heat storage coefficient:

$$C_T = \frac{m'E'}{mE},\ \frac{dT_f}{dz} = g_T\cos\theta - e^{(z-L)L_R}\psi$$

Explicit equation:

$$T_f(z,t) = T_{ebh} - g_T z\cos\theta + \frac{1-e^{-bt}}{L_R}\left[1 - e^{(z-L)L_R}\right]\psi$$

For different wells, the heat storage coefficient can be fitted using test data. Combined with the conservations of mass and momentum in the transient process, the wellbore pressure and temperature coupling model is obtained as follows:

$$\begin{cases} \frac{\partial P}{\partial z} = -\frac{\partial G_m}{\partial t} - \frac{\partial}{\partial z}\left(\frac{\partial G_m^2}{\rho_m}\right) - \rho_m g\sin\theta - \frac{f_m G_m |G_m|}{2d_{ti}\rho_m} \\ T_f(z,t) = T_{ebh} - g_T z\cos\theta + \frac{1-e^{-bt}}{L_R}\left[1 - e^{(z-L)L_R}\right]\psi \end{cases} \quad (8)$$

2.3. Temperature during Production Adjustment

Because production is often unstable, it requires frequent production adjustment. In this case, using an ordinary temperature transient model cannot predict the temperature change accurately, which leads to a large pressure deviation. To improve the prediction accuracy of the real blowout test process, developing the transient superposition correlation of the wellbore temperature is necessary.

Assuming a virtual initial temperature rise time, the temperature is calculated through the steady-state heat transfer model in the period of an increasing production. The temperature change is divided into a superposition of the well shut-in and opening processes in the period of a decreasing production. The corresponding transient superposition is shown in Figure 3.

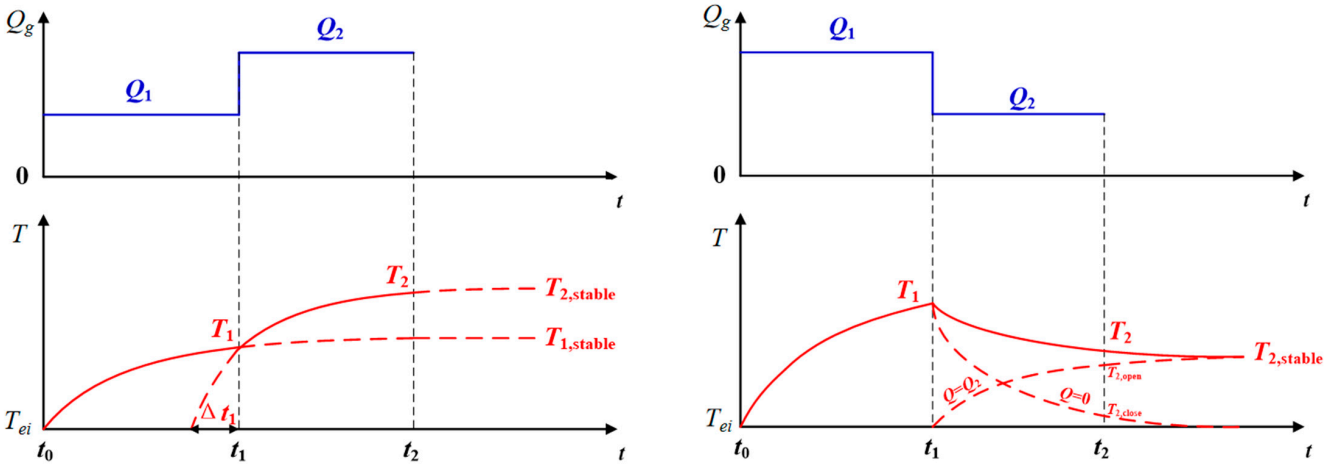

Figure 3. Transient superposition diagram.

(1) Increasing production

The temperature T_1 can be calculated as follows:

$$\frac{T_1 - T_{ei}}{T_{2,stable} - T_{ei}} = 1 - e^{-a\Delta t_1} \tag{9}$$

The virtual time Δt_1 can be calculated as follows:

$$\Delta t_1 = -\frac{1}{a} \ln \frac{T_{2,stable} - T_1}{T_{2,stable} - T_{ei}}$$

Therefore, the temperature T_2 at time t_2 can be calculated as follows:

$$\frac{T_2 - T_{ei}}{T_{2,stable} - T_{ei}} = 1 - e^{-a(t_2 - t_1 + \Delta t_1)} \tag{10}$$

(2) Decreasing production

Temperature changes $\Delta T_{2,close}$ at t_2 time shut-in process can be calculated as follows:

$$\frac{\Delta T_{2,close}}{T_1 - T_{ei}} = e^{-a(t_2 - t_1)} - 1 \tag{11}$$

Temperature changes $\Delta T_{2,open}$ in the well opening process can be calculated as follows:

$$\frac{T_{2,open}}{T_{2,stable} - T_{ei}} = 1 - e^{-a(t_2 - t_1)} \tag{12}$$

Finally, the temperature T_2 at time t_2 can be calculated as follows:

$$T_2 = T_1 + \Delta T_{2,open} + \Delta T_{2,stable} = T_{2,stable} - (T_{2,stable} - T_1)e^{-a(t_2 - t_1)} \tag{13}$$

3. Blowout Test Process and Model Solution

(1) Blowout test process

When the well is closed, the induced fluid is on the top of the test fluid in the wellbore. However, when the gas well is open, the upper induced fluid relieved pressure; wellhead fluid flowed first; and bottom fluid flowed later, leading to a two-phase variable mass flow in the wellbore, the blowout test process is shown in Figure 4. During the upstream period, the gas–liquid fluid flowed from the formation into the wellbore and continuously released heat to the formation and seawater sections. When blown out for a while, a steady

flow stage was developed. Therefore, the transient flow model was coupled by "wellhead nozzle flow + induced fluid pipe flow + well fluid pipe flow + formation seepage."

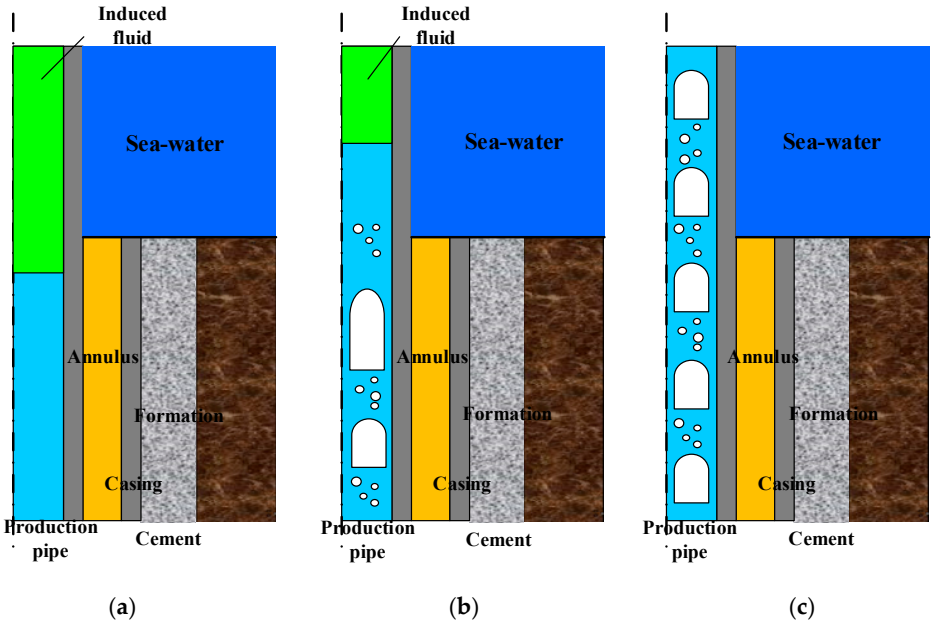

Figure 4. Wellbore flow diagram during the well opening and blowout. (**a**) Before blowout, (**b**) Initial blowout, (**c**) Steady flow.

In summary, based on the above-mentioned phenomena, the two-phase flow transient model comprises the transient conservations of mass, momentum, and energy, and the coupling of the wellbore flow, wellhead throttling, and formation productivity is considered. The influence of the heat transfer difference between the formation and seawater is involved in the calculation of the fluid density in the wellbore using a pseudo single-phase model.

Deliverability equation:

$$q_{gsc} = C\left(P_r^2 - P_{wf}^2\right)^n \tag{14}$$

The flow rate in the blowout was high, and the wellhead nozzle flow was suitable for the multiphase flow formula (i.e., the Sachdeva-Model of subcritical flow).

The critical pressure ratio of gas–liquid two phases passing through the nozzle:

$$p_r = \left\{ \frac{\frac{k}{k-1} + \frac{(1-x_g)v_L(1-p_r)}{x_g v_{g1}}}{\frac{k}{k-1} + \frac{n}{2} + \frac{n(1-x_g)v_L}{x_g v_{g2}} + \frac{n}{2}\left[\frac{(1-x_g)v_L}{x_g v_{g2}}\right]^2} \right\}^{\frac{k}{k-1}} \tag{15}$$

$$n = 1 + \frac{x_{g1}(c_p - c_v)}{x_{g2}c_v + (1-x_{g1})c_l}$$

Total mass flow rate:

$$G_m = CA_2\left[2p_1\rho_{m2}\left(\frac{(1-x_g)(1-p_{rcal})}{\rho_L} + \frac{x_g k}{k-1}(v_{g1} - p_{rcal}v_{g2})\right)\right]^{0.5} \tag{16}$$

(2) Model solution

The transient model of the gas well contains partial differential equations, Equations (1)–(3), which need to be solved numerically. First, divide the well depth H into N sections (the well depth step is $\Delta z = H/N$), and determine the time step Δt and difference grid (Figure 5). The implicit central finite difference method is used to express the difference equations of each grid:

$$f_i(\rho, G) = \left(\rho_{i,j+1} + \rho_{i+1,j+1} - \rho_{i,j} - \rho_{i+1,j}\right) + \frac{\Delta t}{\Delta z}\left(G_{i+1,j} + G_{i+1,j+1} - G_{i,j} - G_{i,j+1}\right) = 0 \tag{17}$$

$$\begin{aligned} f_{N+i}(\rho, G) = {} & \left(G_{i,j+1} + G_{i+1,j+1} - G_{i,j} - G_{i+1,j}\right) + \frac{\Delta t}{\Delta z}\left(\frac{G_{i+1,j}^2}{\rho_{i+1,j}} + \frac{G_{i+1,j+1}^2}{\rho_{i+1,j+1}} - \frac{G_{i,j}^2}{\rho_{i,j}} - \frac{G_{i,j+1}^2}{\rho_{i,j+1}} + p_{i+1,j} + p_{i+1,j+1} - p_{i,j} - p_{i,j+1}\right) \\ & + \frac{\Delta t g \sin\theta}{2}\left(\rho_{i,j} + \rho_{i+1,j} + \rho_{i,j+1} + \rho_{i+1,j+1}\right) + \frac{\lambda \Delta t}{4D}\frac{\left(G_{i,j}+G_{i+1,j}+G_{i,j+1}+G_{i+1,j+1}\right)\left|G_{i,j}+G_{i+1,j}+G_{i,j+1}+G_{i+1,j+1}\right|}{\rho_{i,j}+\rho_{i+1,j}+\rho_{i,j+1}+\rho_{i+1,j+1}} = 0 \end{aligned} \tag{18}$$

where $\rho = \left(\rho_{1,j+1}, \rho_{2,j+1}, \cdots, \rho_{N,j+1}, \rho_{N+1,j+1}\right)$, $G = \left(G_{1,j+1}, G_{2,j+1}, \cdots, G_{N,j+1}, G_{N+1,j+1}\right)$, and $i = 1, 2, \ldots, N$; $i = 1$ represent a wellhead node, and $i = N + 1$ represents a bottom node.

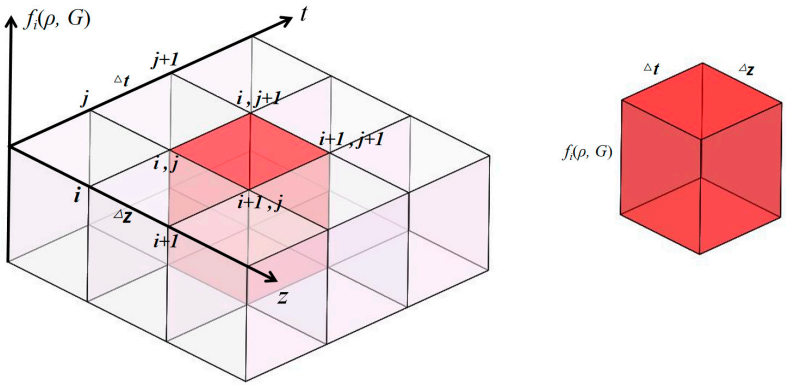

Figure 5. Difference grid of the implicit center finite.

The wellbore pressure at any moment can be solved using the Newton–Raphson method, where the Jacobian matrix J, residual vector R, and independent variable change vector V are, respectively, as follows:

$$J = \begin{bmatrix} 1 & 1 & 0 & \cdots & 0 & 0 & -\Delta t/\Delta z & \Delta t/\Delta z & 0 & \cdots & 0 & 0 \\ 0 & 1 & 1 & 0 & \cdots & 0 & 0 & -\Delta t/\Delta z & \Delta t/\Delta z & 0 & \cdots & 0 \\ \cdots & \cdots & \cdots & \cdots & \cdots & \cdots & \cdots & \cdots & \cdots & \cdots & \cdots & \cdots \\ 0 & \cdots & 0 & 1 & 1 & 0 & \cdots & 0 & 0 & -\Delta t/\Delta z & \Delta t/\Delta z & 0 \\ 0 & 0 & \cdots & 0 & 1 & 1 & 0 & \cdots & 0 & 0 & -\Delta t/\Delta z & \Delta t/\Delta z \\ a_{(N+1)1} & a_{(N+1)2} & 0 & \cdots & 0 & 0 & a_{(N+1)(N+2)} & a_{(N+1)(N+3)} & 0 & \cdots & 0 & 0 \\ 0 & a_{(N+2)2} & a_{(N+2)3} & 0 & \cdots & 0 & 0 & a_{(N+2)(N+3)} & a_{(N+2)(N+4)} & 0 & \cdots & 0 \\ \cdots & \cdots & \cdots & \cdots & \cdots & \cdots & \cdots & \cdots & \cdots & \cdots & \cdots & \cdots \\ 0 & \cdots & 0 & a_{(2N-1)(N-1)} & a_{(2N-1)N} & 0 & \cdots & 0 & 0 & a_{(2N-1)(2N)} & a_{(2N-1)(2N+1)} & 0 \\ 0 & 0 & \cdots & 0 & a_{(2N)N} & a_{(2N)(N+1)} & 0 & \cdots & 0 & 0 & a_{(2N)(2N+1)} & a_{(2N)(2N+2)} \\ a_{(2N+1)1} & 0 & 0 & \cdots & 0 & 0 & 1 & 0 & \cdots & \cdots & 0 & 0 \\ 0 & 0 & 0 & \cdots & 0 & a_{(2N+2)(N+1)} & 0 & 0 & \cdots & \cdots & 0 & 1 \end{bmatrix}_{(2N+2)\times(2N+2)} \tag{19}$$

$$-f_1(\rho, G), -f_2(\rho, G) \cdots\cdots - f_{2N+1}(\rho, G), -f_{2N+2}(\rho, G) \tag{20}$$

$$V = \left[\Delta\rho_{1,j+1}, \Delta\rho_{2,j+1} \cdots\cdots \Delta\rho_{N,j+1}, \Delta\rho_{N+1,j+1}, \Delta G_{1,j+1}, \Delta G_{2,j+1} \cdots\cdots \Delta G_{N,j+1}, \Delta G_{N+1,j+1}\right]^T \tag{21}$$

The Newton–Raphson iterative and Gaussian elimination methods are used to solve the difference equation iteratively. The procedure can be described as follows.

(1) Input basic parameters: well depth H, tubing diameter dti, formation pressure p_r, fluid extraction index I_L, average wellbore temperature T_{ave}, external pressure P_0, nozzle size d_{chock}, test fluid level L_h, and time interval dt.

(2) Calculate the initial values at $t = 0$: bottomhole pressure $p_{wf}(0)$, liquid depth $L_h(0)$, pressure at the liquid level $p_h(0)$, wellhead pressure $p_t(0)$, and liquid column mass $m_L(0)$.

(3) Sort the well structure; determine the calculation step length of the formation and seawater sections; and calculate the position, temperature, and pressure of the interpolation point.

(4) Set the calculation time and calculate the step length; perform the transient flow simulation calculation; and obtain the transient temperature and pressure profiles of the deepwater wellbore.

A simple flowchart of the model solution process is shown in Figure 6.

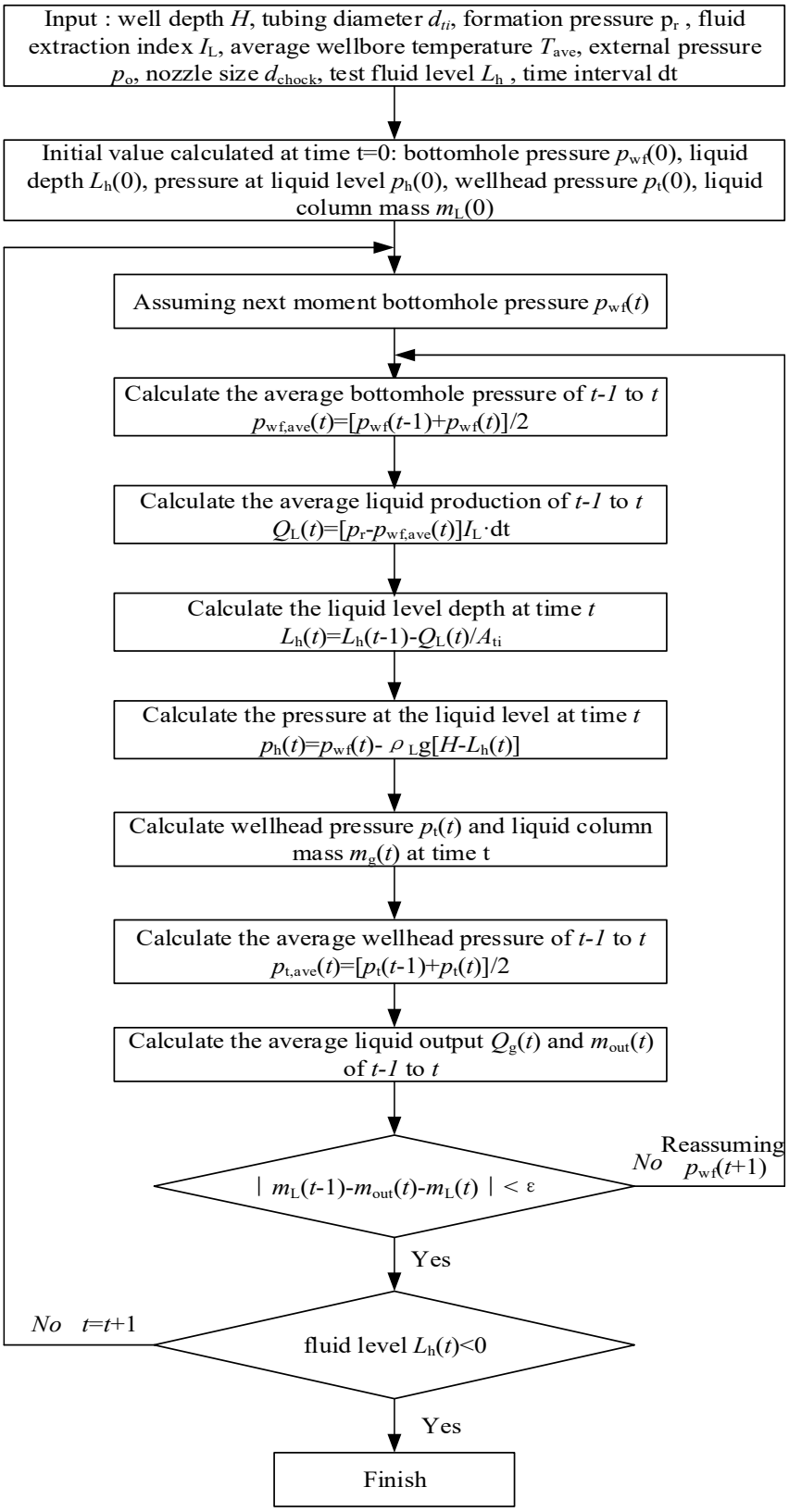

Figure 6. Simple flowchart of the model solution process.

4. Application and Analysis Discussion

We selected deepwater well A to verify the applicability of the established model. The basic parameters corresponding to well A are shown in Table 1.

Table 1. Basic parameters of well A.

Parameter	Value	Unit
Well depth	3350.7	m
Water depth	1447	m
Production pressure	40	MPa
Shut-in wellhead pressure	1.5	MPa
Production temperature	95	°C
Mudline temperature	4	°C
Surface seawater temperature	15	°C
Geothermal gradient	3.87	°C/100 m
Outer diameter of testing pipe	114.3	mm
Inner diameter of testing pipe	76.2	mm
Outer diameter of cement	317.5	mm
Inner diameter of cement	244.5	mm
Heat transfer coefficients of formation section	20	$W/(m^2 \cdot °C)$
Heat transfer coefficients of seawater section	45	$W/(m^2 \cdot °C)$
Formation thermal conductivity	4.2	$W/(m \cdot °C)$
Dimensionless heat storage coefficient	5	-
Induced fluid specific density	1.16	-
Gas specific weight	0.6	-
Hole drift angle	0	rad

Before the blowout, the wellbore was filled with the test and induced fluid. We assumed that the density of the induced fluid was equal to that of the test fluid to simplify the calculation. The gas well productivity is described using an exponential equation; select the coefficient $n = 0.75$ and $C = 1.2 \times 10^4$ $m^3/d \cdot MPa^{-2n}$. The results of the interpolation temperature and initial pressure profile are shown in Figure 7.

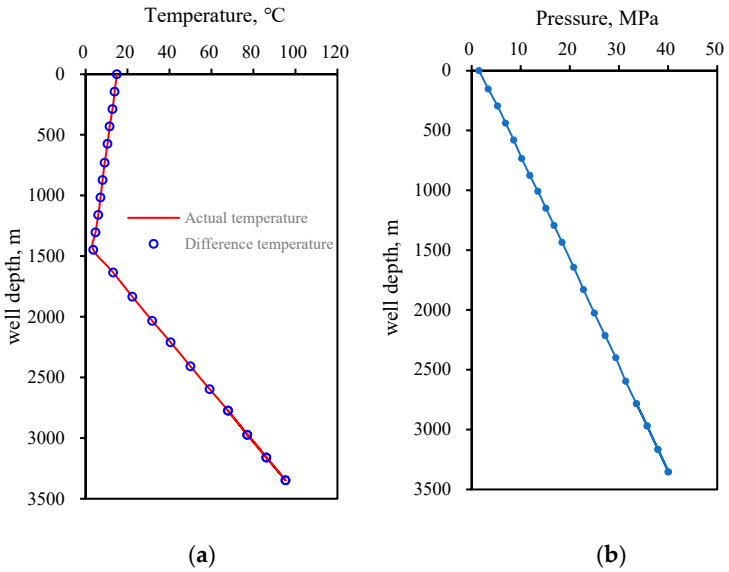

Figure 7. Results of the interpolation temperature and initial wellbore pressure profile. (**a**) Temperature interpolation; (**b**) Initial wellbore pressure.

4.1. Transient Flow Prediction

According to the actual test conditions, the wellbore pressure, temperature, gas production, liquid holdup, hydrate formation temperature, and other parameters were simulated during the blowout (Figure 8). After opening the well for approximately 2 h (8640 s), the formation started producing gas; the working fluid in the wellbore began to be displaced by the gas; the gas–liquid two-phase interface kept moving up; and the wellhead pressure started to increase. At approximately 14,400 s, the wellhead liquid holdup changed to 0 and working fluid was completely displaced, which agreed with the actual situation. The aver-

age error in the wellhead pressure and temperature calculations and measured parameters was less than 5%. The simulations agreed well with the measured values, which showed that the established model met the requirements of computational accuracy. The simulation results were verified via field temperature measurements. The simulation results showed that the mudline temperature was slightly lower than the hydrate formation temperature at the end of the cleanup, and the hydrate inhibitor was injected in the field operation.

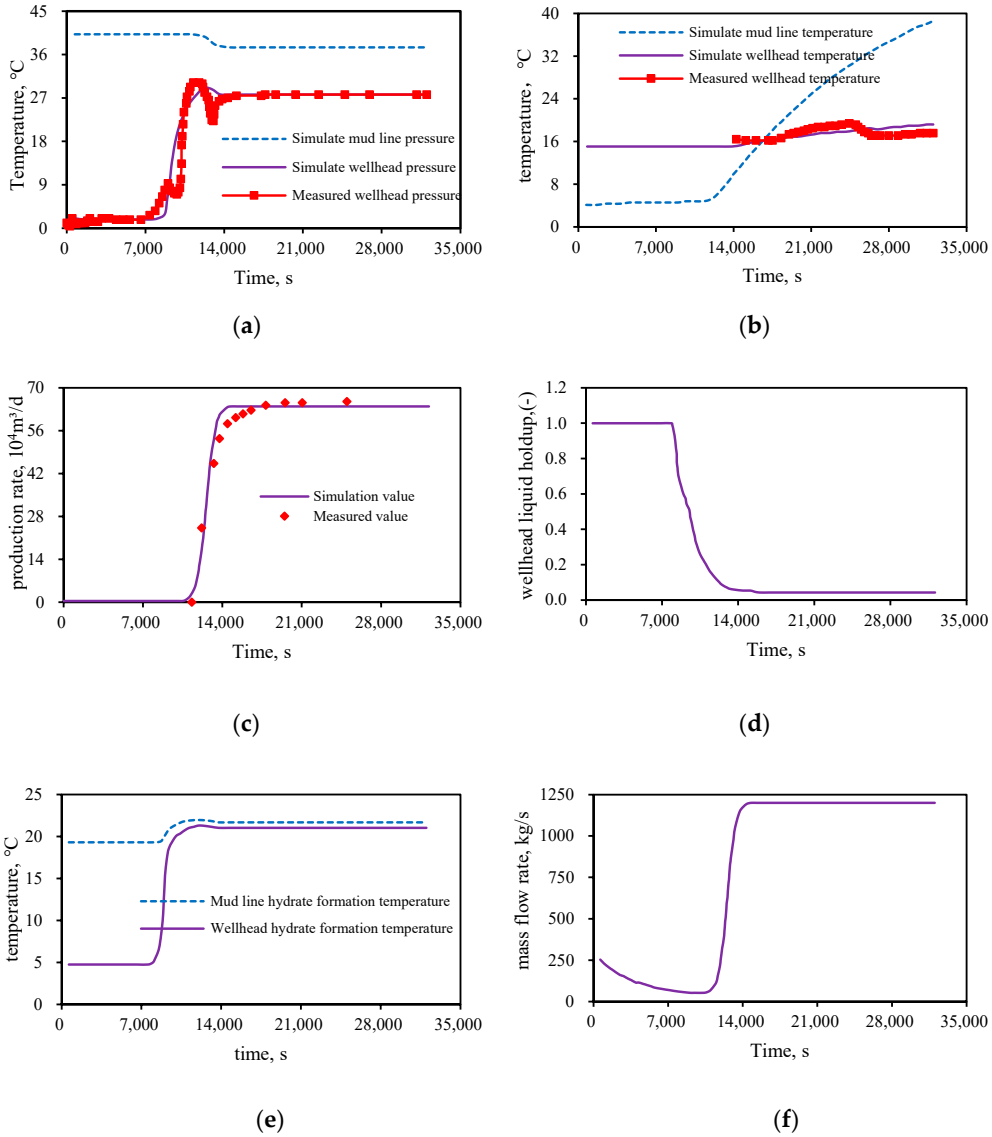

Figure 8. Pressure, temperature, gas production, and liquid holdup simulation of well A. (**a**) Simulation of pressure, (**b**) Simulation of temperature, (**c**) Simulation of gas production, (**d**) Simulation of wellhead liquid holdup, (**e**) Hydrate formation temperature, (**f**) Wellhead mass velocity simulation.

The wellbore pressure, temperature, liquid holdup, and mixture density distribution at different times were predicted; the results are shown in Figure 9. After the well opening, the test fluid was replaced by airflow and wellbore pressure gradient decreased, whereas the wellhead pressure increased gradually. The gas production and wellbore temperature increased gradually. The liquid holdup and mixture density decreased gradually and finally formed as an annular flow.

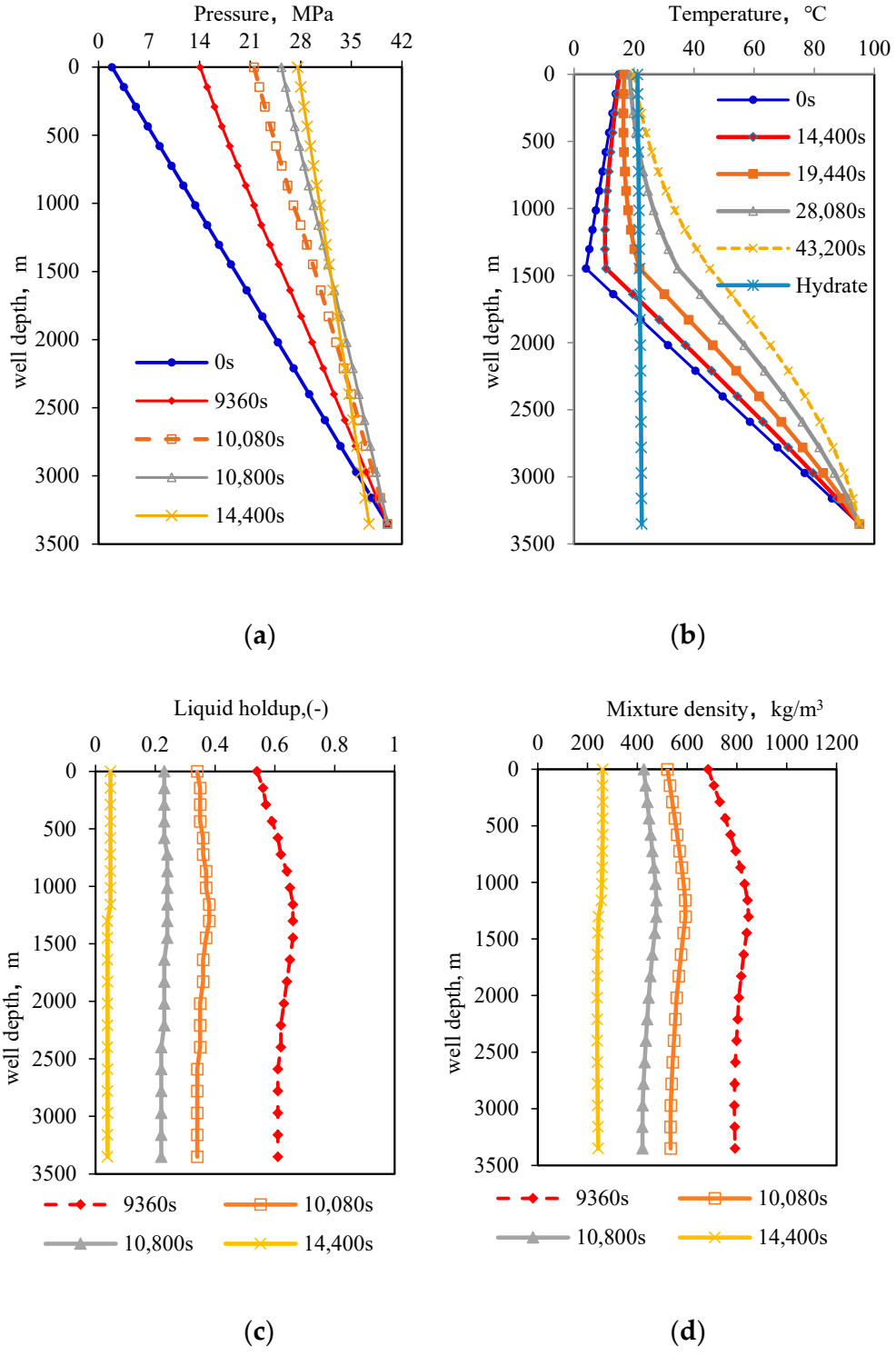

Figure 9. Wellbore pressure, temperature, liquid holdup, and mixture density profiles at different times. (**a**) Wellbore pressure profile, (**b**) Temperature profile prediction, (**c**) Liquid holdup profile, (**d**) Mixture fluid density profile.

4.2. Sensitivity Analysis of the Key Parameters of the Test

(1) Nozzle size

In the blowout design, the nozzle size is an essential technological parameter. The nozzle size significantly influences the clearance time, surface equipment, and flow path. We

selected 3-, 6-, 9-, 12-, and 15-mm nozzles for the sensitivity analysis (Figure 10). The larger the nozzle size, the higher the gas production, the faster the clearance speed, and higher the mudline temperature. When selecting the nozzle size, it should be larger than 10 mm to improve the cleaning speed and mudline temperature as well as prevent hydration.

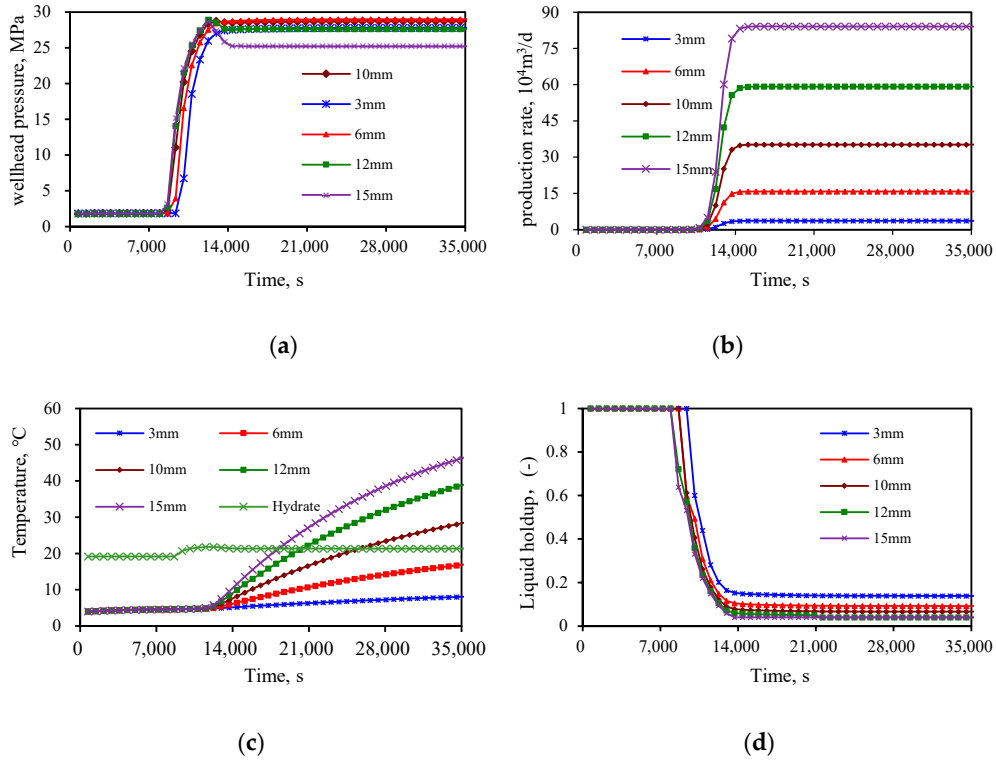

Figure 10. Sensitivity analysis of different nozzle sizes. (**a**) Wellhead pressure (**b**) Gas production, (**c**) Mudline temperature, (**d**) Wellhead liquid holdup.

(2) Influence of tubing sizes

Based on the basic data of well A, 62-, 76-, 88.3-, and 100.5-mm inner diameter tubing were selected for the sensitivity analysis (Figure 11). The larger the tubing, the lower the friction resistance, the higher the gas production, and faster the cleaning speed. However, affected by the decrease in the flow rate, the rising speed of the mudline temperature would be slower. To improve the cleaning speed, choosing tubing with a size of 76 or 88.3 mm is recommended.

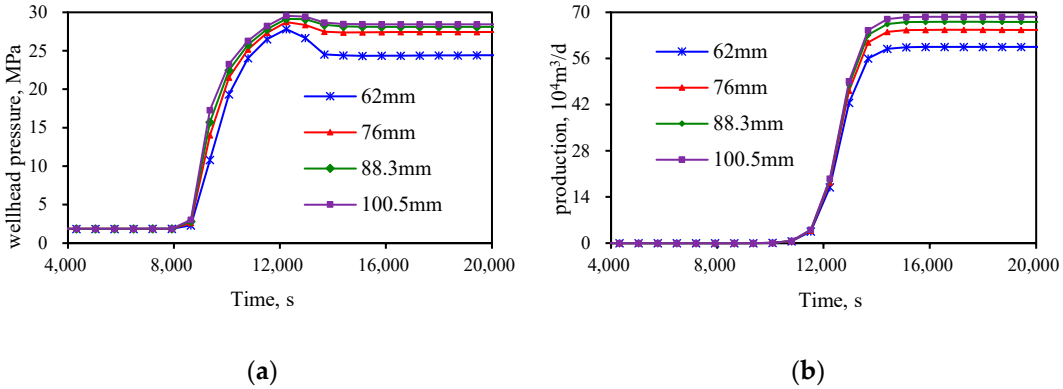

Figure 11. *Cont.*

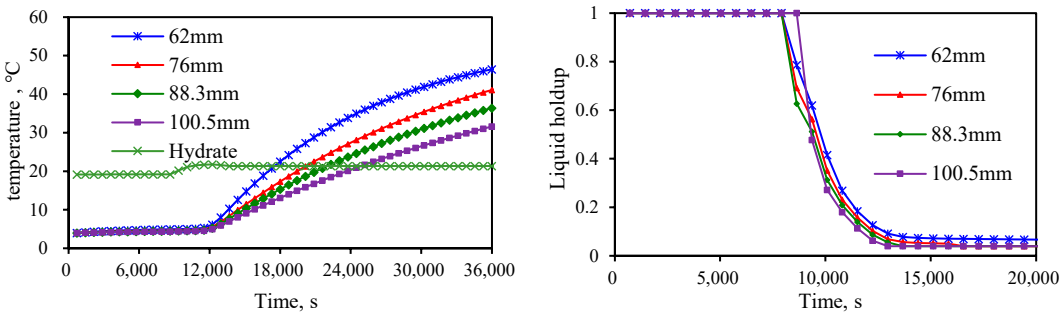

(**c**) (**d**)

Figure 11. Sensitivity analysis of different tubing sizes. (**a**) Wellhead pressure (**b**) Gas production, (**c**) Mudline temperature, (**d**) Wellhead liquid holdup.

5. Conclusions

(1) Coupling formation, wellbore, and surface nozzle flows as well as combining a two-phase nozzle flow model, two-phase fluid holdup model, formation productivity equation, and deepwater transient heat transfer model, a deepwater blowout wellbore transient flow model was established, which considered the characteristics of the transient flow and determines the reliable blowout test time and test system.

(2) As the blowout test continued, the bottomhole pressure decreased slightly and the wellhead pressure increased gradually. Moreover, the wellbore temperature increased gradually; however, the mudline temperature was low. The mudline temperature may be lower than the hydrate formation temperature in the cleaning process, so corresponding measures should be taken to prevent and control the hydrate formation.

(3) The new model can be used to simulate the variation in the wellbore fluid level, pressure, temperature, gas production, liquid holdup, and hydrate formation temperature with time and well depth changing during the blowout period. The simulation result of gas well A showed that the calculated data agreed well with the measured values in the test, with an average error in the wellhead pressure and temperature of less than 5%, and the established model had a high calculation accuracy.

(4) The sizes of the nozzles and tubing are the essential parameters in the blowout design. They significantly influence the clearance time, surface equipment, and blowout process. The transient model of the blowout test in this paper could effectively determine the nozzle regulation system during a blowout test as well as determine the reasonable injection time of the inhibitor and tubing string size. Application analysis and discussion showed that under the condition of satisfying the requirements of the test operation, choosing large nozzle and tubing sizes is necessary to accelerate the discharge of the wellbore working fluid, increase the wellbore temperature, and prevent hydrate formation.

Author Contributions: Data curation, C.Z. and Z.L.; Formal analysis, C.Z.; Investigation, H.Z., M.L. and T.L.; Methodology, H.Z. and T.L.; Project administration, Y.H.; Resources, Y.H. and Z.L.; Validation, C.Z. and M.L.; Writing—original draft, M.L. and C.Z.; Writing—review & editing, H.Z. All authors have read and agreed to the published version of the manuscript.

Funding: National Key R&D Program of China (No. 2021YFC2800905) and National Key Basic Research Development Plan (973 program) "Well completion and test optimization methods for deepwater oil and gas wells": 2015CB251205.

Institutional Review Board Statement: Not applicable.

Informed Consent Statement: Not applicable.

Data Availability Statement: The authors declare that the data of this research are available from the correspondence author on request.

Conflicts of Interest: The authors declare no conflict of interest. The funders had no role in the design of the study; in the collection, analyses, or interpretation of data; in the writing of the manuscript, or in the decision to publish the results.

Nomenclature

A_1~A_{11}	Model coefficient, dimensionless
C_{Jm}	Joule–Thomson coefficient, K/Pa
C_{pm}	Gas–liquid specific heat at constant pressure, J/kg/K
c_p	Gas specific heat at constant pressure, J/(kg·K)
c_v	Gas specific heat at constant volume, J/(kg·K)
c_l	Liquid specific heat capacity, J/(kg·K)
f_m	Two-phase friction coefficient, dimensionless
$f(t)$	Transient heat-conduction time function, dimensionless
GLR	Gas liquid ratio, m^3/m^3
g	Gravitational acceleration, m/s^2
G_m	Two-phase mass flow of per unit area, $kg/(m^2 \cdot s)$
h_r	Convection heat transfer coefficient of annulus fluid, $W/(m^2 \cdot K)$
h_c	Annular fluid radiation coefficient, $W/(m^2 \cdot K)$
h_w	Convective heat transfer coefficient of seawater, $W/(m^2 \cdot K)$
H	Well depth, m
H_f	Fluid enthalpy per unit mass, J/kg
K_e	Formation thermal conductivity, W/(m·K)
k_{cerm}	Cement thermal conductivity, W/(m·K)
Lr	Relaxation distance parameter, m^{-1}
p	Wellbore pressure, Pa
R	Gas constant, 8315 $Pa \cdot m^3 \cdot kmol^{-1} \cdot K^{-1}$
r_{to}	Outer tubing radius, m
r_w	Wellbore radius, m
r_{co}	Outer casing radius, m
t	Time, s
T	Wellbore temperature, K
T_e	Ambient temperature, K
T_{pr}	Pseudo-reduced temperature, dimensionless
U_{to1}	Total heat transfer coefficient of formation, $W/(m^2 \cdot K)$
U_{to2}	Total heat transfer coefficient of seawater, $W/(m^2 \cdot K)$
v_m	Mixture velocity, m/s
w_t	Total mass flow, kg/s
x_g	Gas phase mass fraction, decimal
z	Well depth, m
Z_m	Mixture deviation coefficient, dimensionless
v_L	Liquid specific volume before nozzle, m^3/kg
v_{g1}/v_{g2}	Gas specific volume before/after nozzle, m^3/kg
ρ_m	Two-phase flow density, kg/m^3
ρ_{mr}	Pseudo-reduced density, dimensionless
θ	Angle of inclination, rad
γ_m	Mixture relative density, dimensionless
γ_g	Gas relative density, dimensionless
γ_L	Liquid relative density, dimensionless

References

1. Wang, Y.; Tang, H.; Chen, F. Testing practice and process analysis of high productivity gas Wells in deep water. *J. Oil Gas Technol.* **2009**, *31*, 148–151.
2. Wendler, C.; Maia, C. Planning and conducting well tests in deep and ultra-deep water to mitigate potential risks and justify expense for the operator. In *Brasil Offshore*; SPE-143810-MS; OnePetro: Macaé, Brazil, 2011.
3. Guo, Y.; Sun, B.; Gao, Y.; Zhao, X.; Li, Q.; Zhang, H. Analysis of wellbore flow parameters during shut-in period in deepwater gas well. In Proceedings of the 27th National Symposium on Hydrodynamics, Nanjing, China, 6–8 November 2015; pp. 590–596.

4. Meng, W.; Zhang, C.; Yu, Y.; Ren, G.; Dong, Z. Evaluation to Well Testing Blowout Capability of Deep Water and High Yield Gas Well. *Well Test.* **2015**, *24*, 33–38.
5. Wu, M.; Yang, H.; Liang, H.; Jiang, H.; Chen, M. Key techniques and practices of critical flow based tests for deep water exploration wells: A case study of deep water area in the Qiongdongnan Basin. *Nat. Gas Ind.* **2015**, *35*, 65–70.
6. Churchill, S.W.; Chu, H.H.S. Correlating equations for laminar and turbulent free convection from a vertical plate. *Int. J. Heat Mass Transf.* **1975**, *18*, 1323–1329. [CrossRef]
7. Mathews, K.J. Fluid flow and heat transfer in the top hat oil recovery system. In Proceedings of the SPE Annual Technical Conference and Exhibition, San Antonio, TX, USA, 8–10 October 2012; SPE-160913-STU.
8. Chin, Y.; Wang, X. Mechanics of heat loss in dry tree top-tensioned risers. In Proceedings of the Offshore Technology Conference, Houston, TX, USA, 3–6 May 2004; OTC-16501-MS.
9. Hasan, A.R.; Kabir, C.S.; Lin, D. Analytic Wellbore Temperature Model for Transient Gas-Well Testing. *SPE Reserv. Eval. Eng.* **2005**, *8*, 240–247. [CrossRef]
10. Stiles, D.; Trigg, M.J. Mathematical temperature simulators for drilling deepwater HTHP wells: Comparisons, applications and limitations. In Proceedings of the SPE/IADC Drilling Conference, Amsterdam, The Netherlands, 20–22 February 2007; SPE-105437-MS.
11. Izgec, B.; Kabir, C.S.; Zhu, D.; Hansan, A.R. Transient Fluid and Heat Flow Modeling in Coupled Wellbore/Reservoir Systems. *SPE Res. Eval. Eng.* **2007**, *10*, 294–301. [CrossRef]
12. Izgec, B.; Cribbs, M.E.; Pace, S.V.; Zhu, D.; Kabir, C.S. Placement of Permanent Downhole-Pressure Sensors in Reservoir Surveillance. *SPE Prod. Oper.* **2009**, *24*, 87–95. [CrossRef]
13. Izgec, B.; Hasan, A.R.; Lin, D.; Kabir, C.S. Flow-rate estimation from wellhead-pressure and temperature data. *SPE Prod. Oper.* **2010**, *25*, 31–39. [CrossRef]
14. Ismadi, D.; Kabir, C.S.; Hasan, A.R. The use of combined static-and dynamic-material-balance methods with real-time surveillance data in volumetric gas reservoirs. *SPE Reserv. Eval. Eng.* **2012**, *15*, 351–360. [CrossRef]
15. Spindler, R. Analytical models for wellbore-temperature distribution. *SPE J.* **2011**, *16*, 125–133. [CrossRef]
16. Hasan, A.R.; Kabir, C.S. Wellbore heat-transfer modeling and applications. *J. Pet. Sci. Eng.* **2012**, *86–87*, 127–136. [CrossRef]
17. Kabir, C.S.; Yi, X.; Jakymec, M.; Hasan, A.R. Interpreting Distributed-Temperature Measurements Gathered in Deepwater Gas-Well Testing. In Proceedings of the SPE Annual Technical Conference and Exhibition, New Orleans, LA, USA, 30 September–2 October 2013; SPE-166333-MS.
18. Chen, Z.; Xie, L. Special considerations for deepwater well temperature prediction. In Proceedings of the SPE/IATMI Asia Pacific Oil & Gas Conference and Exhibition, Nusa Dua, Bali, Indonesia, 20–22 October 2015; SPE-176089-MS.
19. Zhou, X.; Duan, Y.; He, Y.; Yuan, Y.; Guo, L.; Ke, D. The Flow Assurance of Deep Water Gas-well Testing. *J. Oil Gas Technol.* **2014**, *36*, 149–152.
20. Zhang, C.; Ren, G.; Dong, Z.; Yi, Y.; Jiang, W. Establishment and application of a wellbore temperature field prediction model for deep water gas well testing. *China Offshore Oil Gas* **2016**, *28*, 78–84.
21. Liu, T.; Zhong, H.; Li, Y. Transient Simulation of Wellbore Pressure and Temperature During Gas-Well Testing. *ASME J. Energy Resour. Technol.* **2014**, *136*, 032902. [CrossRef]
22. Kabir, C.S.; Izgec, B.; Hasan, A.R.; Wang, X. Computing flow profiles and total flow rate with temperature surveys in gas wells. *J. Nat. Gas Sci. Eng.* **2012**, *4*, 1–7. [CrossRef]
23. Tarom, N.; Hossain, M.M. A practical method for the evaluation of the Joule Thomson effects to predict flowing temperature profile in gas producing wells. *J. Nat. Gas Sci. Eng.* **2015**, *26*, 1080–1090. [CrossRef]
24. Li, J.; Guo, B.; Li, B. A closed form mathematical model for predicting gas temperature in gas-drilling unconventional tight reservoirs. *J. Nat. Gas Sci. Eng.* **2015**, *27 Pt 1*, 284–289. [CrossRef]
25. Xu, Z. *Study on Transient Flow Numerical Algorithm and Response Characteristics of Multiphase Flow in Wellbore*; Southwest Petroleum University: Chengdu, China, 2015.
26. He, Y.; Li, Z.; Gao, F.; Zhang, B.; Huang, J.; Li, Y. Simulation of transient flow in deep water gas wells. *Nat. Gas Ind.* **2018**, *38*, 59–64.